Review of Scientific Instruments

RESEARCH ARTICLE | FEBRUARY 03 2021

# Calibration of radiochromic EBT3 film using laser-accelerated protons

M. Ahsan Mahmood ; Seong Geun Lee ; Sang Hwa Lee ; Ha-Na Kim ; Kitae Lee ; Izhar Ahmad; Jeong Moon Yang; Jin Woo Yoon ; Hwang Woon Lee ; Jae Hee Sung ; Seong Ku Lee ; Il Woo Choi ; Chang Hee Nam



*Rev. Sci. Instrum.* 92, 023302 (2021)
https://doi.org/10.1063/5.0031253







AIP Publishing

Review of Scientific Instruments ARTICLE scitation.org/journal/rsi

# Calibration of radiochromic EBT3 film using laser-accelerated protons

Cite as: Rev. Sci. Instrum. 92, 023302 (2021); doi: 10.1063/5.0031253
Submitted: 29 September 2020 • Accepted: 8 January 2021 •
Published Online: 3 February 2021



M. Ahsan Mahmood,[1,2,3] Seong Geun Lee,[1,4] Sang Hwa Lee,[1] Ha-Na Kim,[5] Kitae Lee,[5] Izhar Ahmad,[3] Jeong Moon Yang,[1] Jin Woo Yoon,[1,6] Hwang Woon Lee,[1] Jae Hee Sung,[1,6] Seong Ku Lee,[1,6] Il Woo Choi,[1,6,a)] and Chang Hee Nam[1,4,b)]

## AFFILIATIONS

[1]Center for Relativistic Laser Science, Institute for Basic Science, Gwangju 61005, Republic of Korea
[2]Department of Physics and Applied Mathematics, Pakistan Institute of Engineering and Applied Sciences, Islamabad 45650, Pakistan
[3]National Institute of Lasers and Optronics College, Pakistan Institute of Engineering and Applied Sciences, Islamabad 45650, Pakistan
[4]Department of Physics and Photon Science, Gwangju Institute of Science and Technology, Gwangju 61005, Republic of Korea
[5]Research Center for Ultrafast Science, Korea Atomic Energy Research Institute, Daejeon 34057, Republic of Korea
[6]Advanced Photonics Research Institute, Gwangju Institute of Science and Technology, Gwangju 61005, Republic of Korea

[a)]**Author to whom correspondence should be addressed:** iwchoi@gist.ac.kr
[b)]**Electronic mail:** chnam@gist.ac.kr

## ABSTRACT

We present a proof of principle for onsite calibration of a radiochromic film (EBT3) using CR-39 as an absolute proton-counting detector and laser-accelerated protons as a calibration source. A special detector assembly composed of aluminum range filters, an EBT3 film, and a CR-39 detector is used to expose the EBT3 film with protons in an energy range of 3.65 MeV–5.85 MeV. In our design, the proton beam is divided into small beamlets and their projection images are taken on the EBT3 film and the CR-39 detector by maintaining a certain distance between the two detectors. Owing to the geometrical factor of the configuration and scattering inside the EBT3, the areal number density of protons was kept below the saturation level of the CR-39 detector. We also present a method to relate the number of protons detected on the CR-39 in a narrow energy range to protons with a broad energy spectrum that contribute to the dose deposited in the EBT3 film. The energy spectrum of protons emitted along the target normal direction is simultaneously measured using another CR-39 detector installed in a Thomson parabola spectrometer. The calibration curves for the EBT3 film were obtained in the optical density range of 0.01–0.25 for low dose values of 0.1 Gy–3.0 Gy. Our results are in good agreement with the calibrations of the EBT3 film that are traditionally carried out using conventional accelerators. The method presented here can be further extended for onsite calibration of radiochromic films of other types and for a higher range of dose values.



## I. INTRODUCTION

Acceleration of ions from the interaction of an intense laser pulse and a target has been an active research[1,2] due to its potential applications in fields of proton radiography,[3] clinical oncology,[4,5] neutron generation,[6] and fast ignition.[7] Protons have been accelerated up to nearly 100 MeV using PW class lasers,[8] while several tens of MeV are routinely being generated with 100 TW lasers. Protons accelerated in the so-called target normal sheath acceleration (TNSA) mechanism have a wide energy spectrum with a cutoff energy.[9] In the laser-driven acceleration of protons, a considerable number of other ions with different charge states and other radiations such as electrons and x rays are also generated.[10] For applications requiring energy selectivity, protons with a broad range of energies are desirable, but at the same time, it is necessary to characterize such beams in terms of angular and spectral distribution of

protons. For applications of laser-accelerated proton sources, especially in radiation therapy, it is very important to correctly calculate the dose deposited by protons.[11]

In diagnostics of laser-accelerated ions, an energy-dispersive equipment, based on a combination of electric and/or magnetic fields, coupled with a detection and imaging device is used. The Thomson parabola spectrometer (TPS) equipped with a microchannel plate (MCP) and a charge-coupled device (CCD) is an active real-time diagnostic. Such a detection setup is only able to detect a fraction of the proton beam since a collimating pinhole, used to enhance the spectral resolution of the spectrometer, may significantly restrict the measured region on the beam. Alternatively, layers of energy range filters and passive detectors, such as radiochromic films (RCF), Columbia Resin 39 (CR-39), and imaging plates, are used in a stacked configuration for proton imaging spectroscopy.[12,13] Such a configuration of layered materials uses the inherent properties of protons, i.e., energy deposition in the material. Although this method gives low spectral and spatial resolutions, it is capable of detecting the whole cross-sectional profile of the proton beam and is insensitive to electromagnetic pulses generated during the intense laser-matter interactions.[14]

RCFs are in use for radiation dosimetry[15] in radiation physics and clinical applications owing to their low cost and usability. When exposed to an ionizing radiation, the color of active layer in the film changes and the optical density (OD) related to the absorbed dose can be measured after digitizing the film with an optical scanning system such as a densitometer or a flatbed scanner. For the characterization of laser-accelerated protons, different types of RCFs in a stacked configuration are usually placed in the beam path, and protons deposit their energy in different layers depending on their energy deposition in RCF layers. Measured dose distribution is extracted from OD variations in successive layers that give the spectral and angular distribution of proton numbers.[13] RCF is also sensitive to other background radiations such as x rays and electrons that are produced together with the laser-accelerated protons. An absolute particle-counting detector, CR-39, is a solid-state nuclear track detector that can detect ions with energies as low as 20 keV/nucleon[16] and is insensitive to electrons, x rays, and gamma rays. Since each proton produces an individual pit on CR-39, it can be used to estimate the absolute number of particles. In laser-accelerated proton experiments, CR-39 has been used as a reference detector for the calibration of other detectors, such as MCP used in a TPS.[17] CR-39 requires a time-consuming process of etching and counting the pits, while due to its high sensitivity, it sufferers from saturation at a high fluence of protons.[18] Because of these characteristics, RCF and CR-39 detectors have been complementarily used for spectral characterization of laser-accelerated proton beams in various experiments.[13,19,20]

Due to batch-to-batch differences in RCF manufacturing, the response variation in optical scanners[21] and aging effect of RCF, it is necessary to calibrate the films before their use in absolute dosimetry. When RCFs are used as detectors of laser-accelerated protons, they are usually calibrated using protons from a medical linear accelerator or a conventional accelerator with known energy and absolute numbers.[19,22–24] Feng *et al.*[19] reported the calibration of GAFCHROMIC EBT3 and HD-V2 films at high dose levels using 20 MeV protons from a cyclotron facility. Borca *et al.*[22] studied dosimetric characterization of the EBT3 film in the range of 0.1 Gy–7 Gy for IMRT (Intensity Modulated Radiation Therapy) using photons from a medical linear accelerator. Vallières *et al.*[23] have used low energy protons from a tandem linear accelerator and presented a semiempirical parametric model for calibration of EBT-XD films. Castriconi *et al.*[24] compared the calibration of EBT3 using protons and carbon ions with clinical MeV-photons and electron beams. Although proton beams from a conventional accelerator are monoenergetic and calculation of dose is straightforward in such a case, but it is a cumbersome job to access a separate accelerator facility for the calibration purpose. On the other hand, laser-accelerated protons have a broad energy range and are generated in high numbers, and to the best of our knowledge, there has been no attempt to calibrate RCF using a laser-accelerated proton source. It is also known that due to a high value of the stopping power of the proton in the so-called Brag peak region, there is a quenching effect due to recombination of free electrons that results in under response of RCF, which gives rise to an uncertainty of nearly 15% in dose measurement with protons.[25] For the detection of protons, there is a significant difference in sensitivities of the EBT3 film and CR-39 detector. When used in a stack configuration, for the usual values of OD on the EBT3 film, the corresponding number density of protons detected on CR-39 is very high and it is not possible to count the number of pits formed by individual protons on CR-39. Therefore, in order to relate the measurements of the two detectors, an optimum fluence of protons should be used.

In this paper, we present a proof-of-principle method for onsite calibration of the GAFCHROMIC EBT3 film using CR-39 as an absolute particle-counting detector and laser-accelerated protons as a calibration source. EBT3 was chosen owing to its low dose detection range. The response of the EBT3 film was measured for low OD values of 0.01–0.25 with a corresponding dose range of 0.1 Gy–3.0 Gy, and the extrapolation of fitted data was used to extend the response curves to a high dose range. We presented a model to calculate the effective dose absorbed in RCF by using the proton number density detected on CR-39 and the proton spectrum measured simultaneously using TPS. We compared our results with previously published calibration curves for the EBT3 film[22,24] and found reasonable agreement. It is expected that with a more sophisticated arrangement of energy range filters, CR-39 and RCF, this work can be extended for onsite calibration at higher values of OD as well. This paper is divided into five sections: After introduction in Sec. I, configuration of the detector assembly and the experimental setup are explained in Sec. II. Model calculations for the dose absorbed in the EBT3 film are given in Sec. III, results are discussed in Sec. IV, and the conclusion is presented in Sec. V.

## II. CONFIGURATION OF DETECTION SETUP

EBT3 films are usually used for radiation dosimetry in a range of low dose of 0.1 Gy–20 Gy. It consists of a 28 $\mu$m thin active layer, containing a dye marker and other additives that are sensitive to ionizing radiations, sandwiched between two protective polyester layers of 128 $\mu$m each. In the present scheme of the experiment shown in Fig. 1(a), the "calibration detector assembly" comprising aluminum

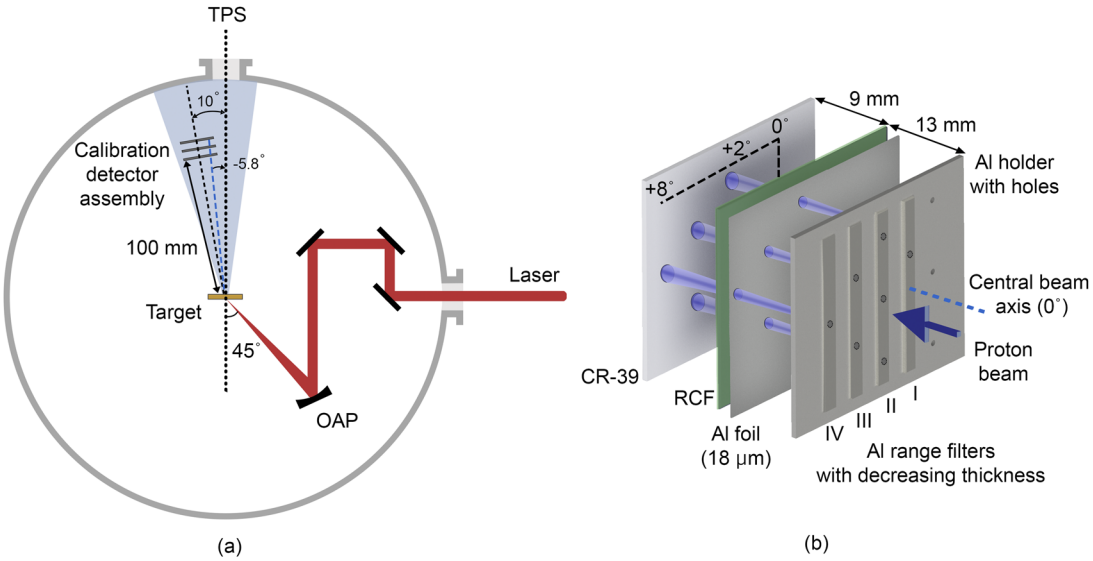


**FIG. 1.** (a) Schematic of the experimental layout used to calibrate the radiochromic film (EBT3) using a laser-accelerated proton source. The calibration detector assembly was positioned at 100 mm from the proton source with an angle of 10° from the target normal direction. The proton beam was emitted with a central axis of the beam making an angle of −5.8° from target normal, shown with a blue dashed line. OAP stands for the off-axis parabolic mirror and TPS stands for the Thomson parabola spectrometer. (b) Arrangement of the calibration detector assembly is composed of Al range filters, Al foil, RCF, and CR-39. Aluminum range filters of 100 $\mu$m, 50 $\mu$m, 36 $\mu$m, and 18 $\mu$m were used at positions of I, II, III, and IV. The central axis of the proton beam (defined as 0°) is shown with a dashed blue line and the beamlets are projected from +2° to +8°.



range filters, the EBT3 film (GAFCHROMIC), and the CR-39 detector (TASTRACK, Track Analysis Systems Ltd.) in series was put into the proton beam path at a fixed distance of 100 mm from the proton source, making an angle of 10° from the target normal direction. Projection images of the proton beam are produced on the EBT3 and the CR-39 in succession. Figure 1(b) shows the full configuration of the detector assembly. To make a clear one-to-one mapping (or correspondence) between the images on EBT3 and CR-39, a specially designed aluminum holder with an array of holes was installed in front of the calibration detector assembly to produce individual beamlets of protons passing through the holes. The thickness of the aluminum holder was 2 mm and enough to stop all protons and carbon ions produced in the experiment so that those protons incident only on the holes could produce individual beamlets. Energy range filters with different thicknesses were used to filter out low energy protons with high fluence and to select protons with different energy ranges for each beamlet. Range filters were pasted on the aluminum holder in a decreasing order of thickness according to the distance from the central axis of the proton beam. Consequently, the beamlets of protons with different energy ranges are incident on the EBT3 and the CR-39 in succession. The EBT3 film was covered with an additional 18 $\mu$m aluminum foil to protect it from background radiations and was placed at 13 mm downstream from the range filters. After passing through the EBT3 film, protons could travel a certain distance (9 mm) in vacuum and were detected on the CR-39 detector with a reduced areal number density of protons. The areal number density of protons exposed on the CR-39 depends on the distance between the EBT3 and CR-39 due to a geometrical factor introduced. In addition, owing to the scattering of protons by the EBT3 film, the image of proton beamlets on CR-39 is further magnified. This magnification of images of beamlets on CR-39 enabled us to relate measurements of the EBT3 and the CR-39, despite the large difference in their detection sensitivities.

Without the detector assembly in place, the full beam profile of the protons was measured using an RCF at a distance of 105 mm from the target, as shown in Fig. 2(a). High energy protons are emitted at smaller cone angles, and the radial symmetry about the central axis (0°) of the proton beam is maintained. The plot of the normalized OD along the horizontal axis (dotted black line) of Fig. 2(a) is shown in Fig. 2(b). The proton beam is emitted at 5.8° from the target normal direction, as indicated by the peak OD value. This deflection of the protons is associated with a non-thermal phase of acceleration that occurs during the early stage of laser target interaction.[26,27] Although the proton beam is deflected toward the direction of the incident laser pulse, the radial symmetry about the central axis of the proton beam is maintained due to the thermal phase of acceleration that sets in soon after the interaction time of the laser pulse with the target. Hereafter, the central axis (0°) of the proton beam is referred to the direction of 5.8° from the target normal. The beamlets are emitted in a range of angles between 8° and 14° from the target normal direction, i.e., between +2° and +8° from the central axis of the proton beam, as shown in Fig. 1(b). Total energy deposited in the EBT3 film by each beamlet was calculated by summing the energies deposited by all protons included in the beamlet, as a function of their energies, inside the

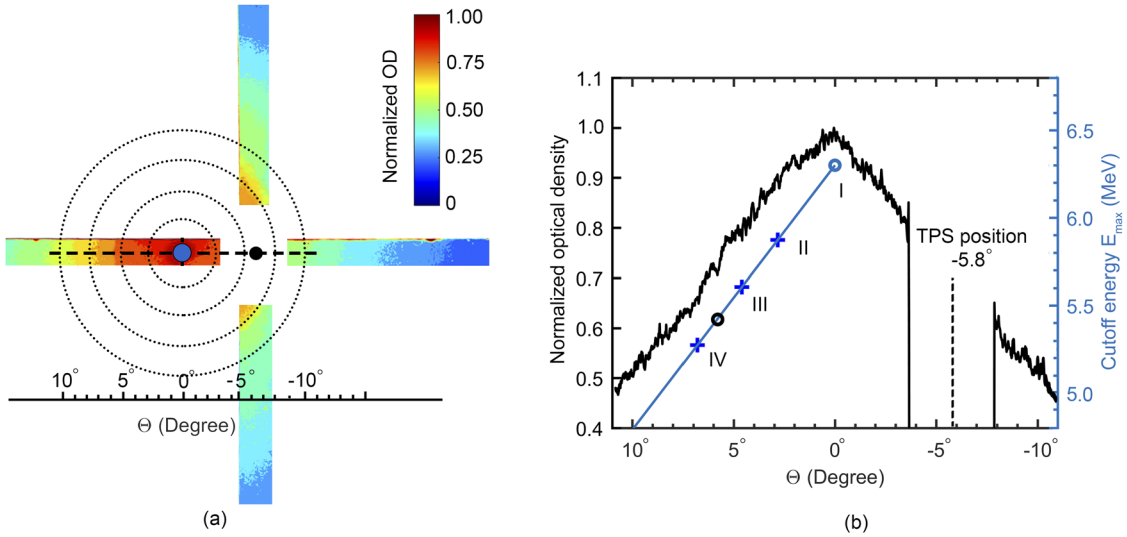


**FIG. 2.** (a) Measurement on a full beam profile of protons measured with another EBT3 film at a distance of 105 mm from the target shows the radial symmetry of the proton beam. The central axis of the proton beam shown in the blue circle is at 0° and the target normal direction is shown with a black circle at −5.8°. Dotted concentric circles are drawn at spacing of 2.5° to show the radial symmetry of the beam profile. (b) Variation of the normalized OD value along the horizontal axis, indicated by the black dashed line in (a). The target normal direction along the TPS is at −5.8° from the central axis of the proton beam. Circles show measured cutoff energy values, while blue crosses, calculated using the interpolation, show the estimated cutoff energy values at three positions along which different beamlets are emitted.

active layer of the EBT3 film. This calculation required absolute number distribution of protons in each beamlet impinging the active layer.

In order to calculate the proton spectra and the cutoff energies in individual beamlets, we utilized the radial symmetry of the proton beam. The spectrum measured using TPS in the target normal direction (−5.8° with respect to the central axis) was scaled to calculate proton spectra in each beamlet. The scaling factor was calculated from the number of high energy protons with a narrow energy range that managed to reach and be detected at CR-39 for each beamlet. The details of the scaling calculations are described Sec. III. The right y-axis in Fig. 2(b) shows the maximum or cutoff energy ($E_{max}$) measured for different beamlets at positions I–IV. The cutoff energy of 5.42 MeV was measured along the target normal direction using TPS. Very few numbers of protons were detected at CR-39 at 0° where a 100 $\mu$m thick aluminum range filter was used in the path of the beam. Therefore, along the central axis of the proton beam, the cutoff energy of 6.30 MeV was calculated using the Stopping and Range of Ions in Matter (SRIM), as shown by the blue circle in Fig. 2(b). Utilizing the radial symmetry of the beam, the cutoff energy at +5.8° from the central axis of the beam [black circle shown in Fig. 2(b)] was assumed to be the same as along the target normal (−5.8°), i.e., 5.42 MeV. Values of cutoff energies, shown by blue crosses, at positions of range filters from II–IV were calculated by interpolating between the values of known cutoff energies, as shown by the blue line in Fig. 2(b).

This experiment was carried out with the 150 TW Ti:sapphire laser[28] installed at the Center for Relativistic Laser Science. The laser system delivered 25-fs laser pulses with a maximum energy of 1.4 J on the target. The temporal contrast of the laser pulse was improved using a double plasma mirror system that provides an ultrahigh contrast laser pulse with contrast ratios better than $10^{11}$ up to 3 ps before the main pulse. The p-polarized laser pulses were focused using an f/3.8 off-axis parabolic mirror (OAP) on targets with an incident angle of 45°, giving a maximum intensity of $2 \times 10^{20}$ W/cm$^2$. The target used in the experiment was a 2-$\mu$m thick Cu foil. The calibration detector assembly was exposed to total 30 laser shots, while proton spectra were measured at the target normal direction by a TPS equipped with a microchannel plate and 16-bit CCD detector for each shot. For the measurement of the absolute number of protons in the beam, a CR-39 plate was installed on a stage at the place of the detector in the TPS setup and was exposed to four laser shots during the experiment.

The exposed EBT3 film was scanned using a flatbed scanner (Epson Perfection V750 Pro) at a resolution of 720 dots/in. in the transmission mode with a 16-bit dynamic range per channel, and then red-green-blue (RGB) images were used to obtain OD values. The OD values obtained with the red channel were used for further analysis because the red channel has been found to be most sensitive due to its higher absorption in the active layer of the EBT3 film.[29] An unexposed EBT3 film was used as a reference and its OD value was subtracted from OD values of the exposed regions to obtain the net OD values. After passing through the aluminum range filter and EBT3 film, protons in a narrow energy range produced pits on the surface of CR-39, which could be seen with an optical microscope after etching for a specific time. The CR-39 was etched in a 6N NaOH solution at 80 °C for 1 h in two steps of 30 min each to monitor the appearance of pits. It was scanned with a microscope (BX53M, OLYMPUS) under 25× magnification. Each image produced by a beamlet was divided into patches of area 0.5 × 0.5 mm$^2$, and a

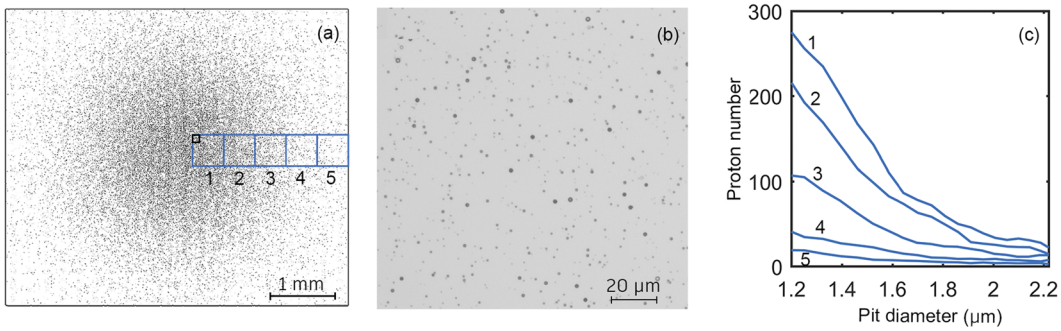


**FIG. 3.** (a) Full image of pits produced by a beamlet of protons, scanned by a microscope (colors are neutralized for visibility). (b) A magnified image of a part of one patch marked with a dark black square in (a). (c) Size distribution of the pit as a function of its diameter in five patches marked with numbers on the central horizontal axis of (a).

particle counting program was used to extract the number of pits on each patch. Figure 3(a) shows the full image of the region exposed by a beamlet on CR-39, and the magnified image of a section of 140 × 140 $\mu m^2$ from a patch is shown in Fig. 3(b). The areal number density of pits is low enough to reliably estimate the number of protons detected at CR-39. For each patch, pits have a size distribution where the number of pits decreases exponentially with size. Distribution of pits on five patches marked in Fig. 3(a) is plotted in Fig. 3(c).

## III. CALCULATION OF DOSE ABSORBED IN RCF

According to our design concept, protons within a certain range of energy (3.65 MeV–5.85 MeV), filtered by the aluminum range filter, deposit their energy in the EBT3 and only high energy protons are able to reach CR-39. Transport of protons from range filters and in the constituent materials of EBT3 and CR-39 was simulated using a Monte Carlo-based program, calculating interaction of ions with matter, SRIM (the Stopping and Range of Ions in Matter).[30] For a given initial energy of one proton particle, the stopping power, i.e., the energy loss per unit path length was integrated to calculate the deposited energy during the transit of a proton in each material layer. We obtained energy deposition per proton, $E_d(E)$, in the active layer of EBT3 as a function of the initial energy, E, for different range filters, as shown with solid lines in Fig. 4. The functional form of $E_d(E)$ shows a rapid increase at a threshold energy $E_i$ and has a peak at $E_0$ and then decreases exponentially with the initial energy. Threshold energy ($E_i$) corresponds to the energy of a proton that manages to reach the active layer of EBT3. $E_0$ is the energy of the proton whose Bragg peak occurs in the active layer and that contributes to maximum energy deposition. $E_i$ was estimated to be 4.25 MeV, 4.00 MeV, and 3.65 MeV, respectively, for an overall thickness of 68 $\mu$m, 54 $\mu$m, and 36 $\mu$m of the aluminum range filters and aluminum foil covering the EBT3 film (18 $\mu$m). On the other hand, threshold energies required to reach the surface of CR-39, $E_{CR}$, were calculated to be 5.70 MeV, 5.50 MeV, and 5.20 MeV for the three aluminum thicknesses, as shown by dashed color lines in Fig. 4. Note that $E_{CR}$ is always larger than $E_i$ due to CR-39 being placed behind EBT3. Protons with initial energies in the range between $E_0$ and $E_{CR}$ are stopped in the second protective layer of EBT3, while protons with the initial energy in the range from $E_{CR}$ to $E_{max}$ arrive at CR-39 with some residual energies. Residual energy is the leftover energy that a proton has after depositing most of its energy in preceding layers of the range filter and EBT3 film. Total energy deposited by a proton before entering CR-39 was calculated by integrating $E_d$ over all material layers preceding CR-39. Then, the maximum threshold energy can be found by subtracting the total deposited energy from the value of $E_{max}$. Values of threshold energies for the EBT3 active layer, CR-39, and estimated cutoff or maximum energies ($E_{max}$) for the filter positions are shown in Table I.

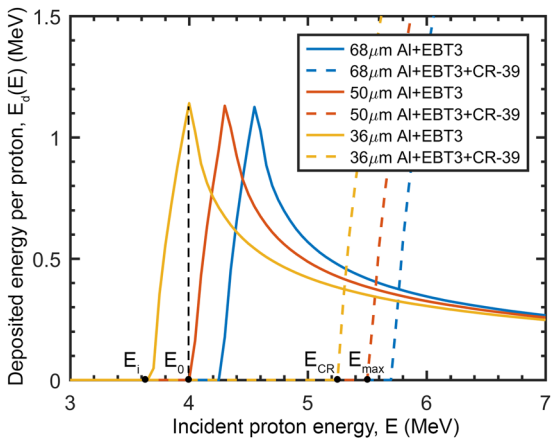


**FIG. 4.** Solid lines show the energy deposition curves in the active layer of EBT3 as a function of initial incident proton energy E for three different range filters with thicknesses of 36 $\mu$m, 54 $\mu$m, and 68 $\mu$m including the thickness of the Al foil that covered EBT3. For clarity, the energies $E_i$, $E_0$, $E_{CR}$, and $E_{max}$ are marked only for the case of the 36-$\mu$m thickness of Al (yellow). Colored dashed lines show the corresponding energy depositions in CR-39. $E_{CR}$ marked in the plot is the threshold energy to reach CR-39, while $E_{max}$ is the maximum or cutoff energy for the case of the 36-$\mu$m thick Al.

**TABLE I.** Threshold energies of a single proton at the active layer of RCF ($E_i$), CR-39 ($E_{CR}$), and the estimated value of cutoff energies ($E_{max}$) for corresponding positions. Total deposited energy after escaping the EBT3 film and the corresponding maximum value of residual energies are also given.

| Filter positions | $E_i$ (MeV) | $E_{CR}$ (MeV) | $E_{max}$ (MeV) | Total $E_d$ deposited after escaping EBT3 (MeV) | Maximum residual energy (MeV) |
|---|---|---|---|---|---|
| II | 4.25 | 5.70 | 5.85 | 5.07 | 0.78 |
| III | 4.00 | 5.50 | 5.60 | 5.05 | 0.55 |
| IV | 3.65 | 5.20 | 5.27 | 4.92 | 0.35 |

Total energy of the proton deposited before reaching the CR-39 and the corresponding value of maximum residual energies are also given.

The available residual energies for different beamlets are in the ranges of 0 keV–780 keV, 0 keV–550 keV, and 0 keV–350 keV depending on the angle of emission. Since the maximum residual energy is below the MeV level for each beamlet, the pits formed by all of the protons are revealed after 1 h of etching for the CR-39. The variation of the pit size depends on the residual energy of protons, and it is known that for protons with sub-MeV energies, the pit size increases with increasing energy.[31–33] Since the number of protons decreases exponentially with energy in the case of the laser accelerated protons and also decreases with the pit size [see Fig. 3(c)], this clearly shows that the pit size increases with energy in the sub-MeV range. At 1 h of etching, variation of the diameter of pits is restricted from 1 ± 0.2 $\mu$m to 2 ± 0.2 $\mu$m[31] for the protons with residual energies in the sub-MeV range (0 keV–780 keV). For each beamlet, the total number of protons per mili-steradian was calculated by integrating the pit distribution on the whole size range divided by the solid angle of the beamlet in mili-steradians. Number of protons $\Delta N_{CR}$ in an energy bin of 100 keV/mSr was calculated using the residual energy range for that beamlet. The error in the estimation of $\Delta N_{CR}$ depends on conditions of scanning on the microscope and also on the error in calculation of the range of residual energies. The value of $\Delta N_{CR}$ was further used to calculate the scaling factor for the estimation of proton spectra for individual beamlets.

Calibrating RCF using a mono-energetic proton source emitted from a conventional accelerator is straight forward because protons contributing to energy deposition in the active layer of RCF exhibit a narrow energy range, where the proton number distribution as a function of energy may resemble a delta function. On the other hand, laser-accelerated protons exhibit a number distribution with a wide energy range (3.62 MeV–5.85 MeV in the present experiment). Total energy deposited by all the protons impinging on the active layer is given by the following integral equation:

$$E_{tot} = \int_{E_i}^{E_{max}} E_d(E) f_N(E) dE, \tag{1}$$

where $E_d(E)$ is the energy deposition in the active layer by a single proton in a certain beamlet and $f_N(E)$ is the absolute number distribution, i.e., the energy spectrum of the incident protons in the same beamlet as a function of the initial energy. Each proton in the energy range from $E_i$ to $E_{max}$ of the number distribution $f_N(E)$ deposits its energy into the active layer of EBT3 with a functional form of $E_d(E)$ shown in Fig. 4. The incident energy spectrum $f_N(E)$ can be deduced from the absolute energy spectrum, i.e., $d^2N/(dE \cdot d\Omega)$ measured with the TPS is proportional to it with a scaling factor $\eta$ given by

$$f_N(E) = \eta \frac{d^2N}{dEd\Omega}, \ \eta = \frac{\Delta N_{CR}}{\Delta N_{Sp}}. \tag{2}$$

The scaling factor $\eta$ is independent of the size of the energy bin or the unit of solid angle. $\Delta N_{Sp}$ is the number of protons at $E = E_{CR}$ per 100 keV/mSr from the spectrum of protons measured in the TPS setup. To calculate the proton spectrum $d^2N/(dE \cdot d\Omega)$, we used another CR-39 to measure the absolute number of protons as a function of energy and installed it at the detector position in TPS[34] in the target normal direction. Four laser shots were accumulated for the exposure on the CR-39 detector by spectrally resolved protons from TPS.

Figure 5 shows the absolute number of protons in the target normal direction in an energy bin of 100 keV/mSr ($d^2N/dE \cdot d\Omega$),

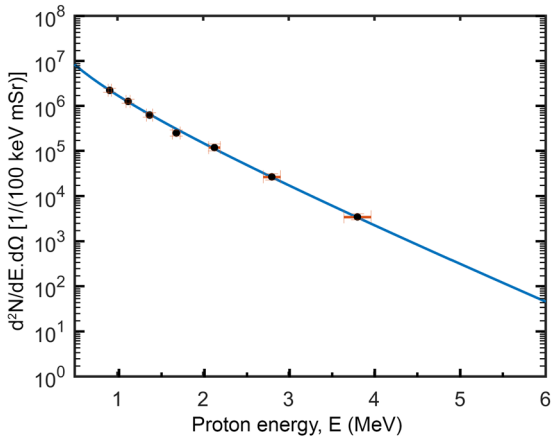


**FIG. 5.** Proton spectrum measured with the CR-39 detector in a TPS. The spectrum was obtained by averaging over the data obtained with four laser shots. The number of protons per 100 keV/mSr ($d^2N/dE \cdot d\Omega$) is plotted on logarithmic scale. Vertical error bars indicate the standard deviation for four laser shots, and horizontal error bars represent the energy dispersion error caused by a collimating pinhole in the TPS.

drawn on a logarithmic scale as a function of proton energy. The value of $d^2N/dE \cdot d\Omega$ was obtained by averaging four datasets measured with the CR-39 detector installed in TPS. Proton number distribution follows an exponentially decaying form with increasing energy. The discrete data of proton numbers are fitted to an assumed Boltzmann distribution,[20,35]

$$\frac{d^2N}{dE \cdot d\Omega}(E) = \frac{N_0}{\Omega E} \exp\left[-\left(\frac{E}{kT}\right)\right], \quad (3)$$

to derive a functional form for the calculation of Eq. (1). Least-square fitting to Eq. (3) gives the values of constants, $N_0 = 1.45 \times 10^6$ and $kT = 0.55$ MeV. $N_0$ is related to the total number of protons in a part of the proton beam that passed through the collimating pinhole installed in TPS, subtending a detection solid angle of $\Omega = 9.5 \times 10^{-8}$ steradian. The slop of the fitted function is related to the temperature of protons. For the calculation of $f_N(E)$, spectral distribution of protons was assumed to remain the same for each laser shot since laser and target parameters were kept the same during this experiment, except negligible shot-to-shot fluctuations in laser energy. It was also assumed that the relative ratio of proton numbers at different energies remains same at the radially symmetric directions around the full proton beam profile, irrespective of the detection solid angle. The scaled proton spectrum $f_N(E)$ for one of the beamlets [marked as zone "2" in Fig. 7(a) in Sec. IV] is plotted in Fig. 6 along with the proton spectrum in the target normal direction measured with TPS. For comparison, the right ordinate shows the corresponding energy disposition function $E_d(E)$ for the EBT3 film and CR-39.

We have used the following procedure to calculate the dose absorbed in the active layer of the EBT3 film. (a) The threshold energy of incident protons $E_{CR}$ required to escape the EBT3 and then be detected at CR-39 was calculated with the SRIM program. (b) The absolute number of protons $\Delta N_{CR}$ corresponding to $E_{CR}$ in an energy interval of 100 keV per mili-steradian was obtained from the number of pits detected at CR-39 and the available range of residual energy in a certain beamlet. (c) The number of protons $\Delta N_{Sp}$ at $E = E_{CR}$ within an energy interval of 100 keV per mili-steradian was calculated from the proton spectrum obtained from TPS measurement in the target normal direction. (d) The scaling factor $\eta$ was determined by taking the ratio of $\Delta N_{CR}$ to $\Delta N_{Sp}$. For each beamlet, $\eta$ was used to calculate the scaled spectra $f_N(E)$ that give the estimated number distribution of protons in a certain beamlet incident on the calibration detector assembly. (e) The total energy $E_{tot}$ deposited in the active layer of EBT3 by all the protons in a beamlet was calculated according to Eq. (1) by integrating the product of the energy deposition $E_d(E)$ and the incident energy spectrum $f_N(E)$ in the range of energies from $E_i$ to $E_{max}$. (f) Total dose D absorbed in the active layer of EBT3 can be calculated by using $D = E_{tot}/\rho AT$. The exposed area ($A = 1.25 \times 10^{-5}$ cm$^2$) corresponding to the unit of scanning resolution for the film, the average density ($\rho = 1.2$ g/cm$^3$), and the thickness ($T = 28$ $\mu$m) of the active layer were used to calculate the total absorbed dose.

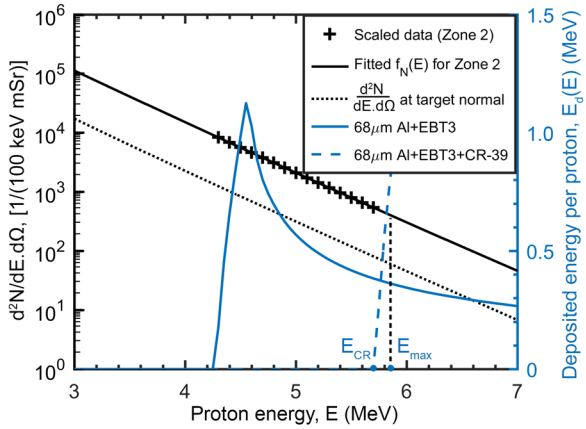


**FIG. 6.** Proton number distribution in a beamlet $f_N(E)$ as a function of proton energy shown as a black solid line. Black crosses represent the calculated data points for protons responsible for the energy deposition in the active layer of the EBT3 film. For comparison, the proton spectrum measured using TPS is shown with a dotted black line. The right ordinate shows the corresponding energy deposition function $E_d(E)$ for EBT3 and CR-39. The values of $E_{CR} = 5.7$ MeV and cutoff energy $E_{max} = 5.85$ MeV are also marked for zone 2 in Fig. 7(a).

## IV. RESULTS AND DISCUSSION

The six different datasets were analyzed to correlate the OD values with the absorbed dose D, obtained at the six different zones in the EBT3 film exposed by the beamlets, as shown in Fig. 7(a). The exposed regions marked as II, III, and IV were covered with a total thickness of 68 $\mu$m, 54 $\mu$m, and 36 $\mu$m of the aluminum filter and foil, respectively. Zone "5" was overexposed by high-energy carbon ions because an open hole was made in the range filter corresponding to this zone. High-energy carbon ions could pass through the 18 $\mu$m aluminum foil covering the EBT3 and made a saturated exposure to zone 5. Among the six datasets, we analyzed five zones, excluding the overexposed zone 5 to further calculate the dose distribution in EBT3. Figures 7(b) and 7(c) show the spatial distribution of OD values at the exposed zone "2" on EBT3.

All five zones were identified on the CR-39 after one hour of etching. They were imaged with an optical microscope under 25× magnification. Each image was divided into small patches with a $0.5 \times 0.5$ mm$^2$ format to count the number of pits, and their number distribution as a function of radius from the center of the image was fitted with the two-dimensional Gaussian function. The number distribution in the patches of zone "2" is shown in Fig. 7(e), while Fig. 7(f) shows the fitted distribution of pit numbers per pixel whose size was matched to the scanning resolution (35.3 $\mu$m, 720 dpi) of the EBT3 film. Since the CR-39 and the EBT3 film were separated by a distance of 9 mm downstream in the proton propagation path, the transverse size of a proton beamlet on the CR-39 is larger than that on the EBT3. The distribution of OD values on EBT3 and that of pit numbers on CR-39 was compared along the horizontal direction to infer the magnification between the two images formed at the EBT3 film and CR-39, and the result is shown in Fig. 7(d). Full widths at $1/e^2$ of the maximum of the distributions were calculated to be $OD_{1/e2} = 2.4$ mm and $N_{1/e2} = 4.09$ mm for EBT3 and CR-39, respectively, and thereby, the magnification factor of 1.7 was obtained. The magnification factor was much larger

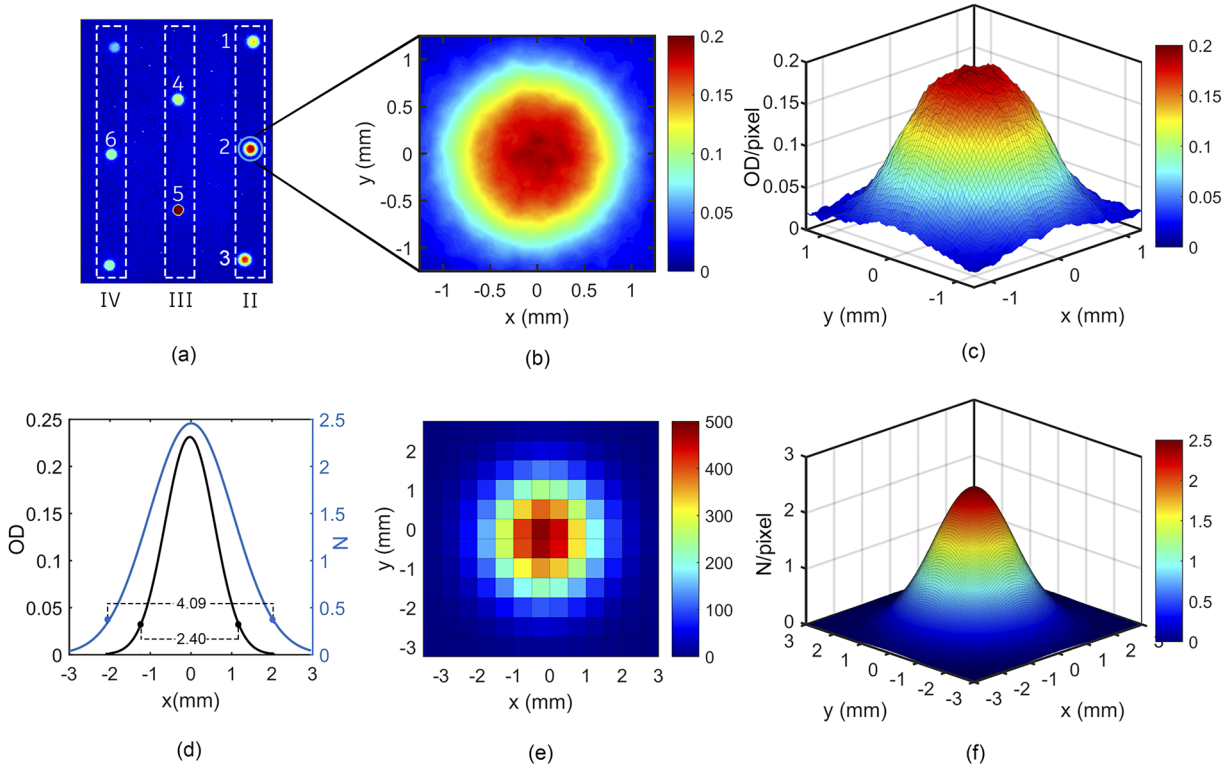


**FIG. 7.** (a) OD profiles on EBT3 scanned using an optical scanner with the red channel. Exposed zones with different range filters are marked with 1–6. (b) and (c) Magnified two-dimensional and three-dimensional plots of the OD value of zone "2." (d) Comparison of the transverse size of the proton beam on EBT3 and CR-39 along the horizontal axis in zone "2." (e) Proton number distribution of zone "2" on CR-39 with a resolution of 0.5 mm. (f) Proton number distribution with the same resolution of 35.3 $\mu$m as that of the optical scanner used for EBT3, obtained with two-dimensional Gaussian fitting to the number distribution of protons shown in (e).

than the geometrical magnification (122 mm/113 mm = 1.08) determined by the positions of EBT3 and CR-39 from the proton source. This may be due to the scattering effect of protons inside the constituent materials of EBT3. We assumed that no particles stray from the proton propagation path, and all the protons passing through the EBT3 film arrive at CR-39. Owing to the larger magnification, we were able to obtain a larger image of the proton beamlet and consequently a relatively lower number density of pits on CR-39, which made the particle counting possible and reliable.

The correlation between the OD values and the absorbed doses of protons was calculated in the five exposed zones shown in Fig. 7(a), and the absolute calibration result of EBT3 is presented in Fig. 8. All data were fitted using a polynomial of the form[36]

$$D = a(\mathrm{OD}) + b(\mathrm{OD})^{n}. \quad (4)$$

To avoid overexposure on CR-39, we were limited to obtain data only for low values of OD in a certain range of 0.01–0.25. For each circular zone in Fig. 7(a), the average OD value per pixel was calculated by dividing the zone in 10 circular strips of increasing radii and taking the average OD in each strip. Similarly, average values of absorbed dose D was calculated by using the proton number distribution [shown in Fig. 7(f)], considering the magnification factor. The calibration data thus obtained and their respective fitted functions, extrapolated to higher OD values, are shown in Fig. 8. Fitting parameters of Eq. (4) are given in Table II. The maximum mean square error of only 0.007 was obtained for fitting the data of zone 1. The energy dispersion error in the measurement of proton spectra can produce uncertainty in the estimation of total dose deposited in the active layer of the EBT3 film. The error in dose calculation has been shown by horizontal error bars in Fig. 8. The mean of the fitted calibrations is depicted as a dotted line, and for comparison, the calibration data reported by Borca *et al.*[22] and Castriconi *et al.*[24] are also shown. The difference in the response curves for different zones is attributed primarily to the uncertainty in the estimation of proton numbers detected on the CR-39 detector. Since proton beamlets with different energy ranges are selected by using range filters, depending on the distance from the central axis of the proton beam, the error in the thickness of range filters and that in the energy dependent scattering of protons inside the range filters and the layers of the EBT3 film also contribute to the differences observed in the response curves for different zones. The averaged curve, however, matches well with previous results for the overall trend of the EBT3 response at a low dose range. The difference from the published data is attributed to the batch-to-batch variation of manufacturing and

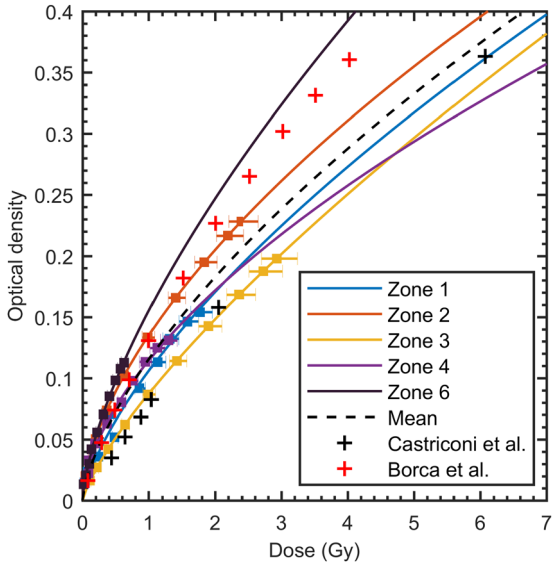


**FIG. 8.** Calibration of EBT3 correlating the absorbed dose D to the optical density OD. Color squares show the measured values of dose in zones 1–4 and 6 in Fig. 7(a). The solid lines present the corresponding fitting curves with a polynomial function [Eq. (1)] of the optical density. The mean of the fitted polynomial functions for five different zones is also shown with a dashed line. Calibration data from Castriconi *et al.* and Borca *et al.* are also plotted for comparison.

**TABLE II.** Values of fitting parameters a, b, and n for the polynomial function, Eq. (4).

| Exposed zone | a | b | n |
|---|---|---|---|
| 1 | 1.72 | 26.33 | 1.55 |
| 2 | 0.31 | 28.14 | 1.69 |
| 3 | 2.12 | 23.30 | 1.38 |
| 4 | 0.23 | 40.90 | 1.72 |
| 6 | 0.35 | 16.02 | 1.52 |

the use of different optical scanners.[29] The maximum value of dose in our calibration was restricted to less than 3.0 Gy since beyond this value, it was not possible to individually count the number of pits on CR-39. It may be possible to extend the calibration to a higher dose by increasing the distance between CR-39 and EBT3 along with using different thicknesses of range filters to select different energy ranges for the protons responsible for the absorbed dose. In addition, the rapid increase in the response at the low dose values requires a precise calibration. The differences also suggest that it is necessary to carry out the calibration of RCF before using these films for the dosimetry purpose, which validates the onsite calibration performed in this study.

## V. CONCLUSION

Calibration of the GAPHCHROMIC EBT3 film was carried out adopting a novel method by using a laser-accelerated proton source and an absolute particle-counting detector CR-39. With an appropriate geometrical configuration of EBT3 and CR-39 in series with respect to the proton source, along with a combination of suitable energy-range filters, we could optimize the absorbed dose on the RCF and the areal number density of pits on the CR-39 detector. This led to correlating the measurements of the two detectors, despite the difference in their detection sensitivities. The proton spectrum measured using TPS was used as a reference for scaling proton spectra at radially symmetric positions in the proton beam. We presented a method to calculate the absorbed dose in the active layer of EBT3 using the laser-accelerated proton source exhibiting a wide range of energies. We utilized the radial symmetry of the proton beam to find the scaling factors to calculate proton spectra for beamlets projecting at different angles. The response of EBT3 was obtained in the dose range of 0.1 Gy–3.0 Gy, and the data were fitted to extend the calibration curves to a higher dose value. The calibration results were compared with the previously reported data, where conventional sources had been used for the calibrations. Our results are found to be in reasonable agreement and validate our method for the onsite calibration of RCF using the laser-accelerated proton source. It is expected that with a novel configuration of the detector assembly, together with a suitable selection of range filters, this method can extend the calibration of RCF to higher dose values. The calibration of RCF is often needed due to batch-to-batch variations in its manufacturing, and it is difficult and time-consuming to calibrate RCFs with a conventional accelerator. This work presented a proof-of-principle method for onsite calibration of RCF using a laser-accelerated proton source. Findings in this work can be applied to proton dosimetry in general and to RCF imaging spectroscopy for laser-accelerated protons.

## ACKNOWLEDGMENTS

The work was supported by the Institute for Basic Science, Korea under the project code, IBS-R012-D1 and by the Ultrashort Quantum Beam Facility (UQBF) operation program through APRI, GIST.

## DATA AVAILABILITY

The data that support the findings of this study are available from the corresponding author upon reasonable request.

## REFERENCES

[1] H. Daido, M. Nishiuchi, and A. S. Pirozhkov, Rep. Prog. Phys. **75**, 056401 (2012).
[2] M. Borghesi, Nucl. Instrum. Methods Phys. Res., Sect. A **740**, 6 (2014).
[3] L. Gao, H. Ji, G. Fiksel, W. Fox, M. Evans, and N. Alfonso, Phys. Plasmas **23**, 043106 (2016).
[4] C.-M. Ma, I. Veltchev, E. Fourkal, J. S. Li, W. Luo, J. Fan, T. Lin, and A. Pollack, Laser Phys. **16**, 639 (2006).
[5] K. Ledingham, P. Bolton, N. Shikazono, and C.-M. Ma, Appl. Sci. **4**, 402 (2014).
[6] A. Favalli, N. Guler, D. Henzlova, S. Croft, K. Falk, D. C. Gautier, K. D. Ianakiev, M. Iliev, S. Palaniyappan, M. Roth, J. C. Fernandez, and M. T. Swinhoe, Sci. Rep. **9**, 2004 (2019).
[7] M. Roth, T. E. Cowan, M. H. Key, S. P. Hatchett, C. Brown, W. Fountain, J. Johnson, D. M. Pennington, R. A. Snavely, S. C. Wilks, K. Yasuike, H. Ruhl, F. Pegoraro, S. V. Bulanov, E. M. Campbell, M. D. Perry, and H. Powell, Phys. Rev. Lett. **86**, 436 (2001).

[8]I. J. Kim, K. H. Pae, I. W. Choi, C.-L. Lee, H. T. Kim, H. Singhal, J. H. Sung, S. K. Lee, H. W. Lee, P. V. Nickles, T. M. Jeong, C. M. Kim, and C. H. Nam, Phys. Plasmas **23**, 070701 (2016).
[9]M. Passoni, L. Bertagna, and A. Zani, New J. Phys. **12**, 045012 (2010).
[10]C. D. Armstrong, C. M. Brenner, E. Zemaityte, G. G. Scott, D. R. Rusby, G. Liao, H. Liu, Y. Li, Z. Zhang, Y. Zhang, B. Zhu, P. Bradford, N. C. Woolsey, P. Oliveira, C. Spindloe, W. Wang, P. McKenna, and D. Neely, Plasma Phys. Controlled Fusion **61**, 034001 (2019).
[11]K. M. Hofmann, U. Masood, J. Pawelke, and J. J. Wilkens, Med. Phys. **42**, 5120 (2015).
[12]C. Scullion, D. Doria, L. Romagnani, H. Ahmed, A. Alejo, O. C. Ettlinger, R. J. Gray, J. Green, G. S. Hicks, D. Jung, K. Naughton, H. Padda, K. Poder, G. G. Scott, D. R. Symes, S. Kar, P. McKenna, Z. Najmudin, D. Neely, M. Zepf, and M. Borghesi, J. Instrum. **11**, C09020 (2016).
[13]M. Schollmeier, M. Geissel, A. B. Sefkow, and K. A. Flippo, Rev. Sci. Instrum. **85**, 043305 (2014).
[14]P. R. Bolton, M. Borghesi, C. Brenner, D. C. Carroll, C. De Martinis, F. Fiorini, A. Flacco, V. Floquet, J. Fuchs, P. Gallegos, D. Giove, J. S. Green, S. Green, B. Jones, D. Kirby, P. McKenna, D. Neely, F. Nuesslin, R. Prasad, S. Reinhardt, M. Roth, U. Schramm, G. G. Scott, S. Ter-Avetisyan, M. Tolley, G. Turchetti, and J. J. Wilkens, Phys. Med. **30**, 255 (2014).
[15]S. Devic, Phys. Med. **27**, 122 (2011).
[16]D. Xiaojiao, L. Xiaofei, T. Zhixin, H. Yongsheng, G. Shilun, Y. Dawei, and W. Naiyan, Nucl. Instrum. Methods Phys. Res., Sect. A **609**, 190 (2009).
[17]R. Prasad, D. Doria, S. Ter-Avetisyan, P. S. Foster, K. E. Quinn, L. Romagnani, C. M. Brenner, J. S. Green, P. Gallegos, M. J. V. Streeter, D. C. Carroll, O. Tresca, N. Dover, C. A. J. Palmer, J. Schreiber, D. Neely, Z. Najmudin, P. McKenna, M. Zepf, and M. Borghesi, Nucl. Instrum. Methods Phys. Res., Sect. A **623**, 712 (2010).
[18]S. Gaillard, J. Fuchs, N. Renard-Le Galloudec, and T. E. Cowan, Rev. Sci. Instrum. **78**, 013304 (2007).
[19]Y. Feng, H. F. Tiedje, K. Gagnon, and R. Fedosejevs, Rev. Sci. Instrum. **89**, 043511 (2018).
[20]F. Nürnberg, M. Schollmeier, E. Brambrink, A. Blažević, D. C. Carroll, K. Flippo, D. C. Gautier, M. Geißel, K. Harres, B. M. Hegelich, O. Lundh, K. Markey, P. McKenna, D. Neely, J. Schreiber, and M. Roth, Rev. Sci. Instrum. **80**, 033301 (2009).
[21]S. N. Chen, M. Gauthier, M. Bazalova-Carter, S. Bolanos, S. Glenzer, R. Riquier, G. Revet, P. Antici, A. Morabito, A. Propp, M. Starodubtsev, and J. Fuchs, Rev. Sci. Instrum. **87**, 073301 (2016).
[22]V. C. Borca, M. Pasquino, G. Russo, P. Grosso, D. Cante, P. Sciacero, G. Girelli, M. R. L. Porta, and S. Tofani, J. Appl. Clin. Med. Phys. **14**, 158 (2013).
[23]S. Vallières, C. Bienvenue, P. Puyuelo-Valdes, M. Salvadori, E. d'Humières, F. Schiettekatte, and P. Antici, Rev. Sci. Instrum. **90**, 083301 (2019).
[24]R. Castriconi, M. Ciocca, A. Mirandola, C. Sini, S. Broggi, M. Schwarz, F. Fracchiolla, M. Martišíková, G. Aricò, G. Mettivier, and P. Russo, Phys. Med. Biol. **62**, 377 (2017).
[25]S. E. Anderson, M. P. Grams, H. Wan Chan Tseung, K. M. Furutani, and C. J. Beltran, Phys. Med. Biol. **64**, 055015 (2019).
[26]K. Zeil, J. Metzkes, T. Kluge, M. Bussmann, T. E. Cowan, S. D. Kraft, R. Sauerbrey, and U. Schramm, Nat. Commun. **3**, 874 (2012).
[27]P. L. Poole, L. Obst, G. E. Cochran, J. Metzkes, H.-P. Schlenvoigt, I. Prencipe, T. Kluge, T. Cowan, U. Schramm, D. W. Schumacher, and K. Zeil, New J. Phys. **20**, 013019 (2018).
[28]J. H. Sung, J. W. Yoon, I. W. Choi, S. K. Lee, H. W. Lee, J. M. Yang, Y. G. Kim, and C. H. Nam, J. Korean Phys. Soc. **77**, 223 (2020).
[29]N. Tagiling, R. Ab Rashid, S. N. A. Azhan, N. Dollah, M. Geso, and W. N. Rahman, Heliyon **4**, e00864 (2018).
[30]J. F. Ziegler, M. D. Ziegler, and J. P. Biersack, Nucl. Instrum. Methods Phys. Res., Sect. B **268**, 1818 (2010).
[31]C. Baccou, V. Yahia, S. Depierreux, C. Neuville, C. Goyon, F. Consoli, R. De Angelis, J. E. Ducret, G. Boutoux, J. Rafelski, and C. Labaune, Rev. Sci. Instrum. **86**, 083307 (2015).
[32]M. Seimetz, P. Bellido, P. García, P. Mur, A. Iborra, A. Soriano, T. Hülber, J. García López, M. C. Jiménez-Ramos, R. Lera, A. Ruiz-de la Cruz, I. Sánchez, R. Zaffino, L. Roso, and J. M. Benlloch, Rev. Sci. Instrum. **89**, 023302 (2018).
[33]A. Malinowska, A. Szydłowski, M. Jaskóła, A. Korman, B. Sartowska, T. Kuehn, and M. Kuk, Rev. Sci. Instrum. **84**, 073511 (2013).
[34]I. W. Choi, C. M. Kim, J. H. Sung, T. J. Yu, S. K. Lee, I. J. Kim, Y.-Y. Jin, T. M. Jeong, N. Hafz, K. H. Pae, Y.-C. Noh, D.-K. Ko, A. Yogo, A. S. Pirozhkov, K. Ogura, S. Orimo, A. Sagisaka, M. Nishiuchi, I. Daito, Y. Oishi, Y. Iwashita, S. Nakamura, K. Nemoto, A. Noda, H. Daido, and J. Lee, Rev. Sci. Instrum. **80**, 053302 (2009).
[35]J. H. Bin, Q. Ji, P. A. Seidl, D. Raftrey, S. Steinke, A. Persaud, K. Nakamura, A. Gonsalves, W. P. Leemans, and T. Schenkel, Rev. Sci. Instrum. **90**, 053301 (2019).
[36]S. Devic, J. Seuntjens, G. Hegyi, E. B. Podgorsak, C. G. Soares, A. S. Kirov, I. Ali, J. F. Williamson, and A. Elizondo, Med. Phys. **31**, 2392 (2004).